Rapid worldwide growth of glacial lakes since 1990

Dan H. Shugar[1,2], Aaron Burr[1], Umesh K. Haritashya[3], Jeffrey S. Kargel[4], C. Scott Watson[5], Maureen C. Kennedy[1], Alexandre R. Bevington[6], Richard A. Betts[7,8], Stephan Harrison[7], Katherine Strattman[3,9]

[1] School of Interdisciplinary Arts and Sciences, University of Washington Tacoma, WA, USA
[2] Present address: Water, Sediment, Hazards and Earth-surface Dynamics (WaterSHED) Laboratory, Department of Geoscience, University of Calgary, AB, Canada *corresponding author daniel.shugar@ucalgary.ca 403-220-5028
[3] Department of Geology, University of Dayton, OH, USA
[4] Planetary Science Institute, Tucson, AZ, USA
[5] COMET, School of Earth & Environment, University of Leeds, UK
[6] British Columbia Ministry of Forests, Lands, Natural Resource Operations and Rural Development, Government of British Columbia, Prince George, BC, Canada
[7] College of Life and Environmental Sciences, University of Exeter, Penryn, Cornwall, UK
[8] Met Office, Exeter, UK
[9] Present address: Department of Atmospheric Science, University of Alabama in Huntsville, AL, USA

Glacial lakes are rapidly growing in response to climate change and glacier retreat. The role of these lakes as terrestrial storage for glacial meltwater is currently unknown and not accounted for in global sea level assessments. Here we map glacier lakes around the world using 254,795 satellite images and use scaling relations to estimate that global glacier lake volume increased ~48%, to 156.5 km^3, between 1990 and 2018. This methodology provides a near-global database and analysis of glacial lake extent, volume and change. Over the study period, lake numbers and total area increased by 53% and 51%, respectively. Median lake size has increased 3%; however, the 95th percentile has increased ~9%. Currently glacial lakes hold about 0.43 mm of sea level equivalent. As glaciers continue to retreat and feed glacial lakes, the implications for glacial lake outburst floods and water resources are of considerable societal and ecological importance.

Keywords: Glacial lakes, sea level rise, climate change, natural hazards

Main

Glaciers are sensitive to climate change[1]. In many locations, enhanced glacier mass loss is supporting the growth of ice-marginal, moraine-dammed, and supraglacial lakes[2–4]. These lakes exist in a variety of forms (e.g. Fig. 25 in[5]) and can accelerate glacier mass loss and terminus retreat ([6–9]) due to calving. Lake-calving glaciers tend to flow more slowly, are less crevassed, and calve less regularly than tidewater glaciers in otherwise similar environments, for reasons that are only partly understood[10]. Further, glacial lake growth, once initiated, can decouple from climate and cause the rapid retreat of glaciers[e.g. 3,11,12], due to a positive feedback as glacial lakes develop adjacent to or at the termini of downwasting glaciers and induce rapid melting. The positive feedback is interrupted when the glacier retreats out of the lake or the lake drains. As glacial lakes drain, they can cause sudden hydrologic and geomorphic change[13–15]. Glacial lake outbursts can pose a risk to people and infrastructure downstream[16–19]. However, some glacial lakes are an economic resource where engineering can mitigate hazards, produce hydroelectric power, and better regulate water outflow[20,21].

While previous work has mapped glacial lake change across individual basins[e.g. 22,23] or regions[e.g. 24–28], no global assessment has investigated glacial lake occurrence or evolution. Recent developments in ‘big data’ cloud computing and geomatics[29,30] have enabled automated mapping that can utilize vast archives of satellite data, yielding a step change in the understanding of global changes to the cryosphere[31].

Glacial lakes temporarily store meltwater, a process that is currently neglected in models addressing glaciers’ hydrological responses to climate change[32] and calculations of sea level rise[33]. Since no global assessment of glacial lake area or volume has previously been undertaken, the volume of water stored in these lakes, and the role of terrestrial interception in modulating global sea level rise, was difficult to estimate; as a result, the temporal trend of glacial lake storage has also been unknown.

Here we quantify glacier lake areas and volumes on a nearly global scale (see red dashed boxes in Fig. 1), using a data cube built from 254,795 Landsat scenes from 1990-2018 using a Normalized Difference Water Index-based model implemented in Google Earth Engine (Methods). The images are aggregated by epoch and verified for complete coverage of glacier proximal areas in order to avoid biases related to differing spatio-temporal image densities. The model identifies and outlines surface water, which is then filtered by a set of variables to retain only glacial lakes (supraglacial, proglacial, and ice-marginal). We then use empirical scaling relations to estimate the total glacial lake volume from measured lake areas to better constrain how terrestrial storage of glacial meltwater is changing decadally and how global sea level is affected. The data also provide a useful benchmark for assessing regional glacial hazards and variability in lake evolution.

The global distribution of glacial lakes

The number and size of glacial lakes have grown rapidly over the past few decades (Figs. 1, 2). In the 1990-99 timeframe (see Methods), 9,414 glacial lakes (>0.05 km^2) covered approximately 5.93x10^3 km^2 of the Earth's surface, which together contained ~105.7 km^3 of water. As of 2015-18, the number of glacial lakes globally had increased to 14,394 (Fig. 1a), a 53% increase over 1990-99. These had grown in total area by 51% to 8.95x10^3 km^2, and their estimated volume increased by 48% to 156.5 km^3 (Fig. 2, Extended Data Figure 1). The median lake size grew at a lower rate, increasing about 3% from 0.129 km^2 in 1990-99 to 0.133 km^2 in 2015-18. The largest lakes also increased in size – the 95th percentile lakes were 1.70 km^2 in 1990-99, and 1.84 km^2 in 2015-18, an estimated increase of ~9%. A Monte Carlo procedure was used to estimate 95% uncertainty prediction intervals for all volume estimates – for total glacial lake volume in 2015-18 this interval is 135.1 to 207.5 km^3. Hereafter, point estimates are provided in the main text, and uncertainty prediction intervals are given in Supplementary Data Table 1. The prediction interval for the difference in global lake volume between 1990-99 and 2015-18 is positive (Extended Data Figure 1), showing that the volume has increased. Over the last quarter century, glacial lake storage increased by ~50.8 km^3 – water that would have otherwise contributed to eustatic sea level rise assuming it did not also feed non-glacial lakes or groundwater aquifers, evaporate, or enter endorheic basins. While lakes often grow as glaciers retreat and the terrain permits, the pattern is less homogeneous along the periphery of the Greenland Ice Sheet, where many ice-marginal lakes drained as ice retreated. Outside of Greenland, the estimated volume of lakes associated with mountain glaciers increased by more than 2/3 from 67.6 km^3 to 113.9 km^3.

The total volume contained in glacial lakes in 2015-18 represents about 0.43 mm of sea level rise equivalent, for an ocean area of 3.625 x 10^8 km^2 (ref [35]). This represents an increase of 0.14 sea level equivalent (SLE) mm since 1990-99. Thus, since the 1990s glacial lakes have intercepted 0.0064 mm a^{-1} of glacier meltwater that would otherwise have contributed to sea level. Bamber et al.[36] indicate that from 2012 to 2016, glaciers and ice caps outside of Antarctica and Greenland lost 227 $\pm$ 31 Gt of ice annually (~248 $\pm$ 34 km^3 of liquid water), contributing 0.63 $\pm$ 0.08 mm a^{-1} of SLE. The Greenland Ice Sheet lost an additional 290 $\pm$ 19 km^3 water equivalent per year from 2003 to 2016, and Antarctica lost 147 $\pm$ 6 km^3 water equivalent annually over the same period[37]. We calculate the annual rates of glacial lake growth (hence, net lake storage of meltwater) based on a 21.5-year span, taking the midpoint of the 1990-99 and 2015-18 periods. Globally, the rate of lake growth means that ~2.36 km^3 a^{-1} of water has been stored in lakes, and excluding Greenland the rate is ~2.15 km^3 a^{-1}. Thus, globally glacial lakes' annual growth and storage of water captures just 0.95% of the net melting of glaciers outside of Greenland and Antarctica, and including the polar ice sheets the fraction is ~0.35%. Globally, this storage term does not represent an important fraction of the hydrological cycle; Messager et al.[38] estimated that all lakes worldwide have a combined volume of 181.9 x 10^3 km^3. The water presently stored in mapped glacial lakes is thus only ~0.1 % of total global lake storage. However, in some mountainous regions, glacial lakes may dominate lake area and volume, and thus contribute disproportionately to the local water cycle. In eastern and central Nepal, for example, all the large lakes are glacial.

Regional lake distribution

Most of the lakes, and especially the largest, are at medium to high latitudes, in Alaska, northern Canada, Scandinavia, Greenland, and Patagonia (Figs. 2, 3). Three Patagonian glacial lakes exceed 1000 km^2 (ref [3]) but volumes for those >200 km^2 (see Methods) were not estimated here (we do report their areas). The (areally) fastest growing lakes, expressed as a percentage, are in Scandinavia, Iceland, and the Russian Federation (Fig. 2a), enlarging 131, 142, and 152% respectively, between 1990-99 and 2015-18. Since many of these lakes are relatively small, their absolute volumetric increases are accordingly not very large (Fig. 2b). For example, lakes in Iceland grew by a total of ~1.5 km^3 to a 2015-18 total of 2.3 km^3, while those in Scandinavia grew by 3.2 km^3 to a 2015-18 total of 5.5 km^3.

Patagonian (not including Lago Argentino, Lago Viedma, and Lago San Martin—named “Lago O’Higgins” in Chile) and Alaskan lakes are growing less rapidly (87 and 80% areal growth respectively), but many lakes in these regions are much larger, resulting in concomitantly large volumetric increases (Fig. 2b). The three very large Patagonian lakes covered about 3,582 km^2 in 2015-18, an increase of about 27 km^2 since 1990-99 (Wilson et al.[3] assessed their areas as 3,682 km^2 in 2016).

Patagonian lakes (excluding the three largest) more than doubled in volume, increasing from ~15.7 km^3 in 1990-99 to 37.2 km^3 in 2015-18 (Fig 3c). By comparison, Loriaux and Casassa[39] estimated an increase in glacier lake storage for the Northern Patagonian Icefield of 4.8 km^3 (to 10.4 km^3) between 1945-2011, with most of the increase occurring since 1987. “Alaskan” lakes (which also include those in Yukon and northwest BC) nearly doubled to 21.4 km^3 (Fig. 3a) since 1990. In Greenland, we observed spatially heterogeneous patterns. On the whole, glacial lakes increased in volume by 12%, containing 42.7 km^3 in 2015-18. While some sectors of Greenland saw substantial increases in lake volume, others experienced large decreases (Fig. 3b). Generally, lakes in the far north and northeast of Greenland are growing very rapidly (Fig 2a) but are relatively small at present. However, Arctic amplification[e.g. 40] may mean that these high latitude lakes are likely to grow rapidly in the coming decades.

While the vast majority of glaciated regions experienced glacial lake growth over the study period, overall, some isolated areas recorded glacial lake reduction. For example, some large lakes fronting Barnes Ice Cap on Baffin Island (western-most blue grid cell in Fig. 2b, and Extended Data Figure 2) partially drained due to frontal retreat of the ice margin between 1990-99 and 2015-18. In southwest Greenland, much of the reduction in lake volume (Fig. 2b) is due to draining of lakes from retreat of the Greenland Ice Sheet. Lakes adjacent to Greenland mountain glaciers on the other hand, generally grew. In some cases, poor quality satellite imagery meant some lakes were not mapped. In the North Coast Ranges of British Columbia for example (blue grid cell in Fig 2a), non-detection of a single large lake resulted in an apparent loss of glacial lake volume overall.

Comparing rates of lake change is relatively straightforward. However, it is difficult to compare our mapping results with other regional inventories, since each study uses different methods and thresholds (see Supplementary Data Table 2 for comparisons between current study and literature). In Patagonia for example, recent efforts[3] mapped 1,401 lakes >0.05 km^2 (excluding the three larger ones) covering 1,135 km^2 in 2016. By comparison, we mapped 1,356 lakes in 2015-18, covering 1,432 km^2.

A statewide inventory of Alaskan glacial lakes has never been undertaken. Post and Mayo's[24] efforts a half century ago included most of the ice-dammed lakes south of the Brooks Range. They mapped 750 >0.1 km^2 lakes in total (including neighbouring Yukon and British Columbia, approximately covering the Randolph Glacier Inventory "Alaska" region), and 538 outside of southeast Alaska (their 'map sheet 2'), covering 540 km^2. Using data from the early 2000s, Wolfe et al.[26] found 204 of Post and Mayo's 'map sheet 2' basins to still be water-filled (115 km^2), and an additional 141 new lakes (13 km^2). Here, we mapped 720 lakes across Alaska (and adjoining Canada) in 2000-04 (covering 820 km^2).

Glacial lakes in HMA (defined as Randolph Glacier Inventory[41] regions Asia South West, Asia South East, and Asia Central) have been studied extensively[e.g., 2,28,30,31]. We find that glacial lakes in HMA are relatively small (Fig. 1, 3d), but are growing rapidly in some subregions (Fig. 2a). Between 1990-99 and 2015-18, the entire region increased in lake volume by ~45%, to 4.6 km^3. Lakes in Asia South East, which encompasses Nepal, northern India, Bhutan, and part of southwestern China, nearly doubled to 2.1 km^3, while Asia South West and Asia Central increased by 18% and 20% respectively. While not a large increase in absolute terms, the increased storage in HMA lakes may heighten the glacial lake outburst flood (GLOF) hazards posed to mountain populations or infrastructure .

In the 'Third Pole' region, Zhang et al.[27] mapped 5,701 lakes (>0.0027 km^2 and within 10 km of a glacier), about 3,800 of which were >0.05 km^2 (see Supplementary Data Table 2). In their database, 4,260 were glacier-fed lakes in 2010, covering a total area of 556.9 km^2, and an increase of ~117 km^2 since 1990. Whereas we mapped 2,037 glacial lakes (>0.05 km^2) in 2010-14, covering a total of 444 km^2. Those lakes grew by ~123 km^2 since 1990-99, increasing by a further 32.2 km^2 by 2015-18.

Several recent studies provide inventories of glacial lake evolution in Nepal. For example, Rounce et al.[18] documented 131 lakes >0.1 km^2 in 2015, of which 91 are <1 km from a glacier. By comparison, we mapped 153 lakes, 89 of which are >0.1 km^2. Rounce et al.[18] found that their 131 lakes grew in area by 9.2% between 2000 and 2015, similar to but slightly less than our findings of 15.6% area growth for 153 lakes.

In the northern Andes, nearly all the glacial lakes are in Peru, but Peruvian lakes contained only 0.58 km^3 of water in 2015-18, an increase of 35% over 1990-99. These may not be growing rapidly in area or volume (Fig. 2) because the majority are moraine-dammed and disconnected from the very steep glaciers feeding them. In other words, the basins are not changing shape as the glaciers retreat further. However, historically the northern Andean glacial lakes have produced numerous GLOFs, so any changes there have an enhanced impact on the risks to local populations[43,44].

In some cases, the new lake growth is concentrated at higher elevations (Fig. 4). For example, we mapped 29 lakes in Bhutan in the 1990s ranging from ~4,303 m to 5,840 m ASL, but 161 in 2015-18, from ~4,159 m to 5,848 m. About two-thirds of the 2015-18 Bhutanese lakes (n=96) were formed at elevations >5,000 m, while there were fewer than one third (n=12) above that elevation in the 1990s. The pattern of increasing lake numbers at higher elevations is not ubiquitous, however. In the Russian Federation, for example, the relatively small number of higher elevation lakes (>1,000 m) have undergone less change, increasing 13% (n=69 in 1990-99; n=78 in 2015-18). Below 1,000 m however, the number of lakes increased 217% (from 290 to 629) over the same period (Fig. 4).

Discussion

This demonstration of a rapid worldwide increase in the number, area, and volume of glacial lakes since the 1990s is attributable to global warming, but other non-climatic drivers also contribute. Specific attribution is difficult, given the complexities of the climatic, glacial, geographic, and topographic variables impacting glacial lakes at regional scales. As a result, we find regional differences in glacier lake growth. The volume of lakes at high latitudes has grown most rapidly, consistent with influences of global warming and associated with Arctic amplification - a universal feature of Global Climate Models[40] and confirmed observationally[45]. Recent instrumental data show that the Arctic has warmed about three times more quickly (mainly in autumn and winter) than the global average[46]. Detailed attribution of expansion of glacial lakes to climate warming would require a clearer understanding of the ways in which glacial lakes evolve, and a model of such processes, as well data on the development of such lakes in the past during an unforced climate. While the difficulties in achieving this are likely high, this would seem to be a priority if we are to better understand future hazards from glacier-lake systems.

One such hazard involves GLOFs, and a recent study[14] maintained that the timing of peak GLOF risk from moraine-dammed glacial lakes incorporates three stages of successive time lags following climate perturbations (warming or drying). These are glacier recession, lake development and expansion, and GLOF triggers. That work suggested that a global GLOF peak (from moraine-dammed lakes) in the 1960s-80s was a delayed response to the glacier recession following the Little Ice Age, and that a future GLOF peak will probably lag by several decades the responses of glacier-lake systems to current warming. Much work has focused on the first step of this process chain (glacier thinning and retreat); our results represent the second stage (glacial lake expansion) and we therefore predict a third stage of increased GLOFs as glacier systems respond to contemporary climate warming.

Besides rising vulnerabilities of human populations in some glacierized mountain ranges, infrastructure for tourism, commerce, and energy security is increasingly exposed to GLOFs. Frequent reassessment of the risks posed by glacier lakes is thus required. Four examples include including tourism, hydropower development, oil/gas pipelines, and highways. (1)

Tourism: The Nepal-side Everest trekking/climbing approach (and the communities that serve it) are exposed to multiple GLOF hazards, including from Imja Lake[2,47], which recently has undergone engineered GLOF hazard mitigation[48]. (2) Hydroelectric power development: In the Himalaya-Karakoram, many hydropower plants exist in, or are exposed to glacial lakes in valleys that have recently experienced GLOFs[17,19]. In some cases, the hydroelectric plants have been destroyed[49,50]. In Peru, Bhutan, Switzerland, and Austria, hydroelectric power development has proceeded in tandem with reduction of GLOF hazards[51]. Glacial lakes can pose opportunities as well as risks; recent work[21] has demonstrated that deglaciated basins may be important storage basins for hydropower development. (3) Petroleum and gas pipelines: The Trans-Alaska Pipeline traverses glacierized mountains that presently contain glacial lakes and may grow new ones with further glacial retreat. The environmental impact statement for the Trans-Alaska Pipeline cited the dynamics of GLOF hazards, where past GLOF behaviour was viewed as insufficient regarding future hazards, emphasizing the need for ongoing assessments[52]. (4) Highways: GLOF hazards also threaten highways that cross glacierized ranges, such as the Karakoram Highway[53] between China and Pakistan[54]; this corridor carries billions of dollars in goods annually and has a regional security aspect.

The growth of a glacial lake does not always convey increased GLOF risk. Most glacial lakes drain slowly or become stable long-term parts of the geography. Some drain suddenly but without consequence either because people and infrastructure are absent, or because settlements and structures are adapted to GLOFs. However, if vulnerabilities are present within a possible GLOF drainage zone and trigger mechanisms exist, then the GLOF risk can be high and may increase with a lake's drainable volume. The worldwide growth in the sizes and number of glacial lakes in populated and developed areas thus should correlate with worldwide GLOF risks[2,5,14,16,18].

Deglaciation is far advanced in places such as the Cordillera Blanca, where total lake volume is small, but the hazards and risks are exceptionally high[e.g. 44,55]. This seeming contradiction is because most glaciers have retreated to cirques, where rock and ice mass can fall off steep slopes directly into the lakes. As deglaciation and lake evolution proceeds in many areas around the world, and as development and exposure to hazards rises, increases in disasters are expected. Conversely, in some mountain regions, as glaciers disappear and lakes drain, or as glaciers and lakes become disconnected, hazards will decrease. In the Bolivian Andes, for example, Cook et al.[56] found a slight decrease in the number of ice-contact glacial lakes between 1986 and 2014, even as the total lake area increased, mostly due to growth of a few larger lakes. They found that ice-marginal (within 500 m) lakes increased notably in both number and area. These were not newly formed, but rather formerly ice-contact lakes that became detached from the glacier(s). Future research should target these regional responses to climate warming.

While many glacial lakes are growing and will likely continue to do so, others may remain quasi-stable, or cease rapid growth due to glacier decoupling or limited accommodation space in overdeepenings[57]. We expect the global trend of glacial lake growth to continue, and perhaps accelerate, in a warming world, as glacier melting and retreat proceeds. Some lakes (especially small ones) may grow more rapidly, while others (especially those becoming decoupled from their glaciers) will no doubt grow more slowly. Others will drain or gradually fill with sediment, or their growth will be stabilized by engineered hazard mitigation. Despite this, these estimates of lake volume changes fill an important knowledge gap in the sea level budget that was noted in the IPCC 5th Assessment Report as well as the US Decadal Survey for Earth Science and Applications from Space[58], and hence help to further increase confidence in understanding and predicting ongoing sea level rise. In addition, the observed changes in glacial lakes will help in future assessments of glacial hazard risk.

References

1. Roe, G. H., Baker, M. B. & Herla, F. Centennial glacier retreat as categorical evidence of regional climate change. *Nature Geoscience* **10**, 95–99 (2017).
2. Haritashya, U. K. *et al.* Evolution and controls of large glacial lakes in the Nepal Himalaya. *Remote Sensing* **10**, 798 (2018).
3. Wilson, R. *et al.* Glacial lakes of the Central and Patagonian Andes. *Global and Planetary Change* **162**, 275–291 (2018).
4. Irvine-Fynn, T. D. L. *et al.* Supraglacial ponds regulate runoff from Himalayan debris-covered glaciers. *Geophysical Research Letters* **44**, 11,894-11,904 (2017).
5. Clague, J. J. & Evans, S. G. *Formation and failure of natural dams in the Canadian Cordillera*. 35 (1994).
6. Warren, C. R. & Kirkbride, M. P. Temperature and bathymetry of ice-contact lakes in Mount Cook National Park, New Zealand. *New Zealand Journal of Geology and Geophysics* **41**, 133–143 (1998).
7. Shugar, D. H., Clague, J. J. & McSaveney, M. J. Late Holocene activity of Sherman and Sheridan glaciers, Prince William Sound, Alaska. *Quaternary Science Reviews* **194**, 116–127 (2018).
8. Chernos, M., Koppes, M. N. & Moore, R. D. Ablation from calving and surface melt at lake-terminating Bridge Glacier, British Columbia, 1984–2013. *The Cryosphere* **10**, 87–102 (2016).
9. Watson, C. S. *et al.* Mass loss from calving in Himalayan proglacial lakes. *Frontiers in Earth Science* **7**, 342 (2020).
10. Truffer, M. & Motyka, R. Where glaciers meet water: subaqueous melt and its relevance to glaciers in various settings. *Reviews of Geophysics* **54**, 220–239 (2016).
11. Bolch, T. *et al.* The state and fate of Himalayan glaciers. *Science* **336**, 310–314 (2012).
12. Trüssel, B. L., Motyka, R. J., Truffer, M. & Larsen, C. F. Rapid thinning of lake-calving Yakutat Glacier and the collapse of the Yakutat Icefield, southeast Alaska, USA. *Journal of Glaciology* **59**, 149–161 (2013).
13. Kershaw, J. A., Clague, J. J. & Evans, S. G. Geomorphic and sedimentological signature of a two-phase outburst flood from moraine-dammed Queen Bess Lake, British Columbia, Canada. *Earth Surface Processes and Landforms* **30**, 1–25 (2005).
14. Harrison, S. *et al.* Climate change and the global pattern of moraine-dammed glacial lake outburst floods. *The Cryosphere* **12**, 1195–1209 (2018).
15. Shugar, D. H. *et al.* River piracy and drainage basin reorganization led by climate-driven glacier retreat. *Nature Geoscience* **10**, 370–375 (2017).
16. Carrivick, J. L. & Tweed, F. S. A global assessment of the societal impacts of glacier outburst floods. *Global and Planetary Change* **144**, 1–16 (2016).

17. Schwanghart, W., Worni, R., Huggel, C., Stoffel, M. & Korup, O. Uncertainty in the Himalayan energy–water nexus: estimating regional exposure to glacial lake outburst floods. *Environmental Research Letters* **11**, 074005 (2016).
18. Rounce, D., Watson, C. & McKinney, D. Identification of hazard and risk for glacial lakes in the Nepal Himalaya using satellite imagery from 2000–2015. *Remote Sensing* **9**, 654 (2017).
19. Byers, A. *et al.* A rockfall-induced glacial lake outburst flood, upper Barun valley, Nepal. *Landslides* **16**, 533–549 (2019).
20. Carey, M. *et al.* Toward hydro-social modeling: Merging human variables and the social sciences with climate-glacier runoff models (Santa River, Peru). *Journal of Hydrology* **518**, 60–70 (2014).
21. Farinotti, D., Round, V., Huss, M., Compagno, L. & Zekollari, H. Large hydropower and water-storage potential in future glacier-free basins. *Nature* **575**, 341–344 (2019).
22. Jha, L. K. & Khare, D. Detection and delineation of glacial lakes and identification of potentially dangerous lakes of Dhauliganga basin in the Himalaya by remote sensing techniques. *Natural Hazards* **85**, 301–327 (2016).
23. Prakash, C. & Nagarajan, R. Glacial lake changes and outburst flood hazard in Chandra basin, North-Western Indian Himalaya. *Geomatics, Natural Hazards and Risk* **9**, 337–355 (2018).
24. Post, A. & Mayo, L. R. *Glacier dammed lakes and outburst floods in Alaska*. 10 (1971).
25. ICIMOD. *Glacial Lakes and Glacial Lake Outburst Floods in Nepal*. (International Centre for Integrated Mountain Development, 2011).
26. Wolfe, D. F. G., Kargel, J. S. & Leonard, G. J. Glacier-dammed ice-marginal lakes of Alaska. in *Global Land Ice Measurements from Space* (eds. Kargel, J. S., Leonard, G. J., Bishop, M. P., Kääb, A. & Raup, B.) 263–295 (Springer Praxis, 2014). doi:10.1007/978-3-540-79818-7_12.
27. Zhang, G., Yao, T., Xie, H., Wang, W. & Yang, W. An inventory of glacial lakes in the Third Pole region and their changes in response to global warming. *Global and Planetary Change* **131**, 148–157 (2015).
28. Chen, F., Zhang, M., Tian, B. & Li, Z. Extraction of glacial lake outlines in Tibet Plateau using Landsat 8 imagery and Google Earth Engine. *IEEE Journal of Selected Topics in Applied Earth Observations and Remote Sensing* **10**, 4002–4009 (2017).
29. Pekel, J. F., Cottam, A., Gorelick, N. & Belward, A. S. High-resolution mapping of global surface water and its long-term changes. *Nature* **540**, 418–422 (2016).
30. Gorelick, N. *et al.* Google Earth Engine: Planetary-scale geospatial analysis for everyone. *Remote Sensing of Environment* **202**, 18–27 (2017).
31. Scherler, D., Wulf, H. & Gorelick, N. Global assessment of supraglacial debris cover extents. *Geophysical Research Letters* (2018) doi:10.1029/2018gl080158.
32. Huss, M. & Hock, R. Global scale hydrological response to future glacier mass loss. *Nature Climate Change* **8**, 135–140 (2018).
33. Church, J. A. *et al. Sea level change*. 1137–1216 (2013).
34. Cook, S. J. & Quincey, D. J. Estimating the volume of Alpine glacial lakes. *Earth Surface Dynamics* **3**, 559–575 (2015).
35. Cogley, J. G. *et al. Glossary of Glacier Mass Balance and Related Terms, IHP-VII Technical Documents in Hydrology No. 86*. (UNESCO-IHP, 2011).
36. Bamber, J. L., Westaway, R. M., Marzeion, B. & Wouters, B. The land ice contribution to sea level during the satellite era. *Environmental Research Letters* **13**, 063008 (2018).
37. Lenaerts, J. T. M., Medley, B., Broeke, M. R. & Wouters, B. Observing and modeling ice sheet surface mass balance. *Reviews of Geophysics* **57**, 376–420 (2019).

38. Messager, M. L., Lehner, B., Grill, G., Nedeva, I. & Schmitt, O. Estimating the volume and age of water stored in global lakes using a geo-statistical approach. *Nature Communications* **7**, 13603 (2016).
39. Loriaux, T. & Casassa, G. Evolution of glacial lakes from the Northern Patagonia Icefield and terrestrial water storage in a sea-level rise context. *Global and Planetary Change* **102**, 33–40 (2013).
40. Serreze, M. C. & Barry, R. G. Processes and impacts of Arctic amplification: A research synthesis. *Global and Planetary Change* **77**, 85–96 (2011).
41. Arendt, A. *et al. Randolph Glacier Inventory – A Dataset of Global Glacier Outlines: Version 5.0*. (2015).
42. Kirschbaum, D. *et al.* The state of remote sensing capabilities of cascading hazards over High Mountain Asia. *Frontiers in Earth Science* **7**, (2019).
43. Carey, M. Living and dying with glaciers: people's historical vulnerability to avalanches and outburst floods in Peru. *Global and Planetary Change* **47**, 122–134 (2005).
44. Kargel, J. *et al.* ASTER Imaging and Analysis of Glacier Hazards. in *Land Remote Sensing and Global Environmental Change: NASA's Earth Observing System and the Science of ASTER and MODIS* (eds. Ramachandran, B., Justice, C. O. & Abrams, M. J.) 325–373 (Springer New York, 2011). doi:10.1007/978-1-4419-6749-7_15.
45. Post, E. *et al.* The polar regions in a 2°C warmer world. *Science Advances* **5**, eaaw9883 (2019).
46. Cowtan, K. & Way, R. G. Coverage bias in the HadCRUT4 temperature series and its impact on recent temperature trends: Coverage Bias in the HadCRUT4 Temperature Series. *Quarterly Journal of the Royal Meteorological Society* **140**, 1935–1944 (2014).
47. Lala, J. M., Rounce, D. R. & McKinney, D. C. Modeling the glacial lake outburst flood process chain in the Nepal Himalaya: reassessing Imja Tsho's hazard. *Hydrology and Earth System Sciences* **22**, 3721–3737 (2018).
48. Kargel, J. S. *et al. The Community Based Flood and Glacial Lake Outburst Risk Reduction Project (CFGORRP)*. 92 http://cfgorrp.dhm.gov.np/wp-content/uploads/2016/03/9.-2015-Feb-UNDP-Imja-FinalReport-13Feb-jsk-commented-31-march-cleaned.pdf (2014).
49. Shrestha, A. B. *et al.* Glacial lake outburst flood risk assessment of Sun Koshi basin, Nepal. *Geomatics, Natural Hazards and Risk* **1**, 157–169 (2010).
50. Khan, Z. Shishper Glacier near Hunza turned into a glacial lake outburst flood yesterday. *Mashable Pakistan* https://pk.mashable.com/science/3394/shishper-glacier-near-hunza-turned-into-a-glacial-lake-outburst-flood-yesterday (2020).
51. Palmer, J. The dangers of glacial lake floods: Pioneering and capitulation. *EOS, Transactions, American Geophysical Union* (2019) doi:10.1029/2019EO116807.
52. United States Department of the Interior. *Final environmental impact statement: proposed trans-Alaska pipeline.* (U.S. Dept. of the Interior; for sale by the Supt. of Docs., U.S. Govt. Print. Off.], 1972).
53. Ashraf, A., Naz, R. & Roohi, R. Glacial lake outburst flood hazards in Hindukush, Karakoram and Himalayan Ranges of Pakistan: implications and risk analysis. *Geomatics, Natural Hazards and Risk* **3**, 113–132 (2012).
54. Bhambri, R. *et al.* The hazardous 2017–2019 surge and river damming by Shispare Glacier, Karakoram. *Scientific Reports* **10**, (2020).
55. Frey, H. *et al.* Multi-source glacial lake outburst flood hazard assessment and mapping for Huaraz, Cordillera Blanca, Peru. *Frontiers in Earth Science* **6**, (2018).
56. Cook, S. J., Kougkoulos, I., Edwards, L. A., Dortch, J. & Hoffmann, D. Glacier change and glacial lake outburst flood risk in the Bolivian Andes. *The Cryosphere* **10**, 2399–2413 (2016).
57. Cook, S. J. & Swift, D. A. Subglacial basins: Their origin and importance in glacial systems and landscapes. *Earth-Science Reviews* **115**, 332–372 (2012).

58. National Academies of Sciences, Engineering, and Medicine. *Thriving on Our Changing Planet: A Decadal Strategy for Earth Observation from Space*. 716 https://doi.org/10.17226/24938 (2018).

Main text figure captions

Figure 1. Near-global glacial lake distribution and evolution. Map of glacial lakes >0.05 km^2 and <200 km^2 in 2015-18, with 1° latitude/longitude summaries. In the map, every circle represents an individual lake. Areas in red dashed boxes (plus Antarctica, not shown) were not mapped due to lack of available imagery. Antarctica (RGI region 19) was omitted because the USGS does not presently provide Landsat data as Surface Reflectance products, which is required for time series analysis from multiple satellite sensors.

Figure 2. Glacial lake volume change (1990-99 to 2015-18). (a) Percent (%) change; and (b) magnitude change (km^3) per 2.5° latitude and longitude bins, with 2.5° latitude/longitude summaries. Volumes computed using a modified version of the empirical area-volume scaling relationship from Cook and Quincey[34].

Figure 3. Regional glacial lake volume changes, 1990-99 to 2015-18. (a) Alaska and western Canada; (b) Greenland and Eastern Canadian Arctic; (c) Patagonia; (d) HMA. Boxes are 2.5° latitude and longitude bins and volume change magnitudes are sums over the period of record. Land masses shown in light grey, and oceans in darker grey.

Figure 4. Histograms of glacial lake elevation (numbers of lakes). Rows are arranged latitudinally.

Methods

Existing literature includes many methods for mapping glacial lakes from remotely sensed data. Here we use a modified Normalized Difference Water Index (NDWI) approach, combined with a variety of thresholds and filters to identify and accurately map glacial lakes across the world. The first section ("Optical Spectral Indices & Raster Analysis) pertains to the initial mapping of water pixels from optical imagery in Google Earth Engine. The second section ("Post-processing and Filtering") describes the filtering of polygons based on a variety of thresholds, performed in ArcGIS Pro. We then describe the scaling relationship used to estimate lake volume from measured area.

Optical Spectral Indices & Raster Analysis

The NDWI[59] is a common approach for mapping water from optical satellite data:

$$NDWI = \frac{GREEN - NIR}{GREEN + NIR} \tag{1}$$

where NIR is the Near Infrared band. In the mountains, cloud cover, steep terrain, and highly variable water reflectivity (for example due to sediment, seasonally frozen lake water, and icebergs) render the use of NDWI more challenging[e.g. 60]. Nie et al.[61] described an object-oriented image processing approach where they combine NDWI and a Normalized Difference Snow Index (NDSI) (equation 2) to derive individual glacial lake outlines, and then a series of steps including edge-based segmentation algorithms to refine the classification.

$$NDSI = \frac{GREEN - SWIR1}{GREEN + SWIR1} \qquad (2)$$

where SWIR is the Shortwave Infrared 1 band. Several methods taking advantage of the greater spectral resolution of Landsat-8 (compared with earlier Landsat satellites) have recently been proposed to map glacial lakes. Bhardwaj et al.[60], for example, threshold a ratio of pan-sharpened bands 1 (coastal/aerosol) and 9 (cirrus cloud), filter for temperature (using Landsat-8 thermal band 10), and for slope using a digital elevation model. While this approach returns impressive results and is well-suited for future hazards assessments, it is not as useful for historic analyses since Landsat-8 (and thus the coastal/aerosol and cirrus bands) has been operational only since 2013, and the higher-resolution pan band is only available on Landsat-7 and -8. Further, since the panchromatic band records over the visible wavelengths only, it can distort the spectral characteristics of the multispectral bands, especially NIR[62]. As a result, pan-sharpening should typically be reserved for the purposes of visualization of visible bands.

While the free access to the Landsat archive has revolutionized Earth science[63], the acquisition rates and spatial resolution of other satellite sensors have increased dramatically in recent years, thus enabling improved time series analysis for the more recent periods and extension of the analysis to smaller lake sizes[e.g. 64].

Some authors[e.g. 60] have mapped lakes by carefully selecting individual satellite images and using spectral indices, as above. While this labor-intensive image selection is reasonable for small areas, it is not suitable for global analyses. As a result, a method is required that automatically selects imagery at global scales.

Google Earth Engine is a relatively new platform that harnesses cloud computing to analyse massive quantities of geospatial data[29,30], especially raster imagery. The entire Landsat, Sentinel-1 and -2, ASTER, and MODIS data archives are available for rapid processing without the need for downloading any imagery to a local computer.

Here, we describe a method for mapping glacial lakes that combines attributes of previous methods and allows historic analyses as far back as 1982 (Landsat-4 Thematic Mapper), depending on cloud-free image availability. Our method involves computing and thresholding NDWI and NDSI on every input image, then mosaicking and filtering for a variety of variables (Extended Data Figure 4).

We stacked calibrated surface reflectance data from 254,795 individual scenes from Landsat missions 4, 5, 7, and 8 to produce a multi-sensor data cube. Since NDSI uses the SWIR1 band, we could not use Landsat missions prior to Landsat-4. We restricted the cube to relatively (typically <20%, see below) cloud-free scenes from the ablation season, so as to minimize the likelihood of snow and a frozen lake surface. The ablation season was updated empirically for each region depending on the local melt season (which was adjusted based on an iterative interpretation of the mosaic), while the cloudiness was determined from the scene metadata, and was typically set to 20% except in cases where no imagery was available for a particular region for a particular time (Supplementary Data Table 3). While some scenes were available from 1982-1989, large data gaps prevented a global analysis. As a result, we restricted our time series to 1990-2018. In a few Arctic regions (Svalbard, Jan Mayen, Franz Joseph Land) insufficient cloud-free scenes existed for a thorough analysis, and so those areas were not analyzed for any time period. We also did not map areas in RGI region 19 (Antarctica, which includes small island groups, e.g., the Kerguelen Islands and South Georgia). Antarctica was omitted because the USGS does not (at present) provide Landsat data as Surface Reflectance products, which is what was used for all other regions. Surface reflectance data accounts for atmospheric effects such as aerosol scattering and thin clouds, which is necessary in time series analysis between sensors. We cannot use Top of Atmosphere data (which is available for Antarctica). Recent work however, has used Landsat and Sentinel 2 satellites to map thousands of supraglacial lakes across Antarctica[65] in a single melt season. Similarly, researchers are leveraging Google Earth Engine to analyze daily changes of supraglacial lakes across Greenland using MODIS[66]. Though the gap areas in our analysis are few, for purposes of filling in the inventory, we urge contributions from the scientific community using new tools and data as they become available.

We then calculated NDWI and NDSI for each scene in the cube, and averaged the cube pixel-wise to produce a mosaic where pixel values represent the proportion (0-1) of scenes that meet or exceed a threshold, which were determined empirically for each region independently. For example, for a cube 10-scenes deep, where a particular pixel's NDWI exceeded the threshold value seven times, the resultant mosaic pixel value for the NDWI band would be 0.7. The thresholds were determined iteratively by adjusting the values, running the script, and visually comparing the mapped lake with the optical image mosaic for that time step.

We produced a threshold for the mosaic pixel-wise based on NDWI, NDSI, red band (a proxy for brightness), surface temperature (from the thermal band), slope, and elevation (from input digital elevation model (DEM), see below). Since glacial lakes should be warm relative to the snow or ice sometimes surrounding them, we used a threshold of >-1°C. This reduces the likelihood that relatively flat, shadowed snowy slopes are included in the lake polygon, since they tend to be colder than our threshold of -1°C. The pixel-wise slope threshold was set high, typically to 40º. Without this step, some lakes that were adjacent to very steep, snow-covered shadowed cirques and arêtes became artificially large since they included many false positive snow pixels. In some regions at extreme latitudes where glaciers and ice caps are often located on relatively flat terrain, we relaxed this threshold (see Supplementary Data Table 3). We later filtered for median lake slope using a much lower threshold. One drawback to filtering for slope on a pixel-wise basis is that pixels covering the former margins of glaciers (e.g. reflecting when the DEM was constructed) are typically filtered out, since they are steep. As a result, some lakes were artificially bisected. The mitigation of this problem is described in the next Methods section.

The elevation threshold was set to 5 m ASL, so as to reduce the likelihood of classifying ocean water as lake. Many coastal waters, particularly in Alaska and Greenland, have inaccurate elevations in the DEM (see below about DEM selection). In parts of coastal Greenland for example, ocean pixels in some fjords have a DEM elevation of 5 m, and are often classified as 'lake' (see example false positives in Kangerlussuatsiaq Fjord, Extended Data Figure 8b). A 5 m threshold has the drawback of filtering out true lakes (or parts thereof) that are <5 m ASL (e.g. Malaspina Lake, Alaska). At the global scale however, the downside of a relatively small number of false negatives outweighs a much higher number of false positives. To minimize the number of false positives, we removed many of these manually (in ArcGIS Pro) following automatic processing in Google Earth Engine and ArcGIS Pro. But the aim of this analysis was to produce a uniform lake database and so do as little manual intervention as possible.

Since the DEM (combination of ASTER GDEM2 and GMTED2010, see 'Sources of Error' section, below) represents the Earth's surface at a different time from the input satellite imagery, it is incorrect in areas that have experienced substantial change, including on glaciers. In many tidewater glacier settings therefore, the DEM over what is now ocean represents a glacier surface and is therefore too high. As a result, we produced false positives in some tidewater environments. While the goal of this paper is not to heavily manually edit the lake polygons, we do in the case of false positives over the ocean since they can be very large (10s km^2) and so influence regional statistics.

For recent years (typically >~2000), annual mosaics were often possible. In earlier years however, insufficient satellite coverage, or poor-quality imagery (e.g. due to heavy cloud cover, snow and frozen lake surfaces, and terrain shadows) meant that multi-year mosaics were necessary. For consistency, we produce 5-year mosaics beginning on the full and half decade (e.g. 2000, 2005, 2010, and 2015), except in the 1990s when relatively few scenes were available. For that decade, we produce decadal mosaics (1990-99). We did not produce 1980s mosaics because of data incompleteness as described above. The 2015 mosaic contains scenes from 2015-2018. Producing multi-year mosaics has several benefits, as well as some drawbacks. Most importantly, image 'noise' (e.g. small icebergs and brash ice, SLC-off striping[67], haze, etc) is reduced. The main cost of doing a 5-year mosaic is that areas experiencing rapid glacier retreat, and often rapid lake change, will be characterized by a somewhat 'blurred' glacier margin. For some regions at extreme latitudes, very few scenes were available, even in recent years. We have noted these cases where no mosaic was produced in Supplementary Data Table 3.

The threshold (binary) image of water pixels was then vectorized and exported to ArcGIS Pro and a set of further filtering steps was undertaken.

Post-Processing & Filtering

Often, individual pixels within a lake did not satisfy the thresholds described above, and left gaps. In some cases, these gaps bisected a lake, leaving two lakes instead of one. To mitigate this issue, and to account for incorrect lake boundaries due, for example, to icebergs, in ArcGIS we dilated (buffered) all polygons by 45 m (1.5 pixels), merged touching polygons, and then contracted the polygons by 45 m to return as closely as possible to the original configuration but with correctly merged lakes. This has the undesirable effect of scalloped polygon edges, and in rare cases truly isolated and closely adjacent lakes may be falsely merged into one, but this is considered minor compared with the benefit of coalescing incorrectly split lakes.

Since lakes are flat, we filtered for the median slope ($\leq$10°) of all pixels enclosed by the polygon based on the DEM. In other words, as described above we earlier filtered on a pixel-wise basis for a higher gradient, but then again filtered the median lake slope for a lower gradient. Water polygons were then filtered for size (0.05 to 200 km^2). We chose 0.05 km^2 as a lower limit because smaller thresholds produced many false positives. A lower limit of 0.05 km^2 was considered a reasonable tradeoff. For the upper size limit, while no 200 km^2 lakes exist in our test areas (explained below), large lakes exist in Patagonia and Alaska, so we set this limit high. In Patagonia, some lakes exceed 1000 km^2; however, lakes of this size are unrepresented in the volume-area scaling dataset (see below) and so we do not include them in our volume assessment. The only lake >200 km^2 that was included is one in Patagonia that was <200 km^2 early in the time series. We kept it as filtering it out partway through the time series would imply the lake had disappeared when it fact it had grown. If the very large Patagonian lakes (Lago Argentino, Lago Viedma, Lago San Martin) were counted in our analysis, then Argentina would likely top the list of country-level lake data (e.g. Extended Data Figure 3). We do however, include their areas. Future studies should work towards collecting high-resolution bathymetric datasets of these very large lakes so we can better understand whether they represent a different population, from a volume-area perspective.

We then performed a spatial intersection with the GLIMS/Randolph Glacier Inventory (v6.0) glacier database[41,68], keeping only lake polygons that are within 1 km of a glacier polygon. For Greenland, we combined GLIMS (which includes only the outlet glaciers) with the IMBIE/Rignot database (http://imbie.org/imbie-2016/drainage-basins/), which also includes the ice sheet. The 1 km buffer captures lakes that recently (probably within the last few decades) detached from glaciers due to glacial retreat[e.g. Fig 3c in 11], as well as larger supraglacial lakes that are persistent enough to be visible on multiyear mosaics. To track individual lakes through time, we assigned a geocoded ID based on the latitude and longitude of the lake centroid. We processed all regions outside of Antarctica and interior Greenland (we did analyze coastal Greenland), to produce a near-global assessment of glacial lake occurrence and evolution.

Error Assessment - glacial lake mapping

To demonstrate the methodology, we produced pixel-wise mosaics for test areas in High Mountain Asia (HMA) and southwest Greenland. These two regions are characterized by very different physiography (topography, climate), and the method performed relatively well, and relatively poorly, respectively, in them. The HMA mosaic was built from 29 Landsat-7 and -8 scenes from 2016-17 over an area encompassing the Everest region of eastern Nepal and adjoining Tibet (China) (Extended Data Figure 5). In Extended Data Figure 6, we show results from the various processing steps outlined in Extended Data Figure 4. Visually, the agreement between the automated and manual mapping is excellent, though there are lakes that were missed with the automated detection. We discuss the sources of error below.

For coastal southwest Greenland, we produced a mosaic from 30 Landsat-8 scenes from 2016-17 over an area surrounding Kangerlussuatsiaq Fjord and Maniitsoq ice cap (Extended Data Figure 7). This area was chosen to contrast with the High Mountain Asia region, because the model performed relatively poorly in the coastal environment.

In our HMA test area, 140 glacial lakes were manually digitized (Extended Data Figure 6), ranging from 0.05 to 3.89 km^2, with a median (and standard deviation) size of 0.14±0.45 km^2, and totaling 41.18 km^2. The automated digitizing returned 130 lakes ranging from 0.05 to 3.89 km^2, with a median of 0.16±0.48 km^2, and totaling 41.91 km^2. The vast majority of lakes identified manually and by the automated spectral index methods are small (<0.25 km^2), but manual digitizing produced slightly more (n=98) of the smallest lakes than did the automated methods (n = 87; Extended Data Figure 6).

In our Greenland test area, 35 glacial lakes were manually digitized (Extended Data Figure 8, 9), ranging from 0.05 to 2.08 km^2, with a median size of 0.21±0.42 km^2, and totaling 12.33 km^2. The automated digitizing returned 36 lakes ranging from 0.05 to 2.04 km^2, with a median of 0.27±0.43 km^2, and totaling 13.82 km^2. As in HMA, the majority of lakes identified manually and by the automated spectral index methods are small (<0.5 km^2).

We quantified mapping error in two ways. For each error assessment method, we compared the optical-generated lake polygons against the manually digitized lake outlines, which we consider to contain fewer errors than the automatically mapped outlines. Parameters for optical mapping for our HMA error analysis region included per-scene NDWI and NDSI thresholds (0.1 and 0.5, respectively), average (mosaicked) thresholds of 0.4 and 0.3 respectively, and DOY range (120-300, or approximately May to October inclusive, for 2016-17). All optical data were from Landsat-7 and -8. For the Greenland study area, our NDWI and NDSI thresholds were 0.2 and 0.4 respectively, with average (mosaicked) thresholds of 0.3 and 0.5 respectively, and DOY range (150-300). All optical data were from Landsat-8.

First, we compared the area calculated for each auto-digitized lake polygon with the area of the same lake by manual digitizing (Extended Data Figure 9). Since all lakes were assigned an ID based on the coordinates of their centroid, we can be confident that we are comparing the same lake using the different methods. In some cases, the centroid was not the same and as a result, the coordinate ID differs, which we discuss below.

The second method of error analysis is an Image Classification Accuracy Assessment (Supplementary Data Table 4, 5), where we compared a classified image (auto-generated lake polygons for the HMA and Greenland test regions) to another data source that is considered to be accurate (manually digitized lake polygons). This was done via a set of random points ($5x10^4$ for each test region), with a resulting confusion matrix (aka error, or correlation matrix), which reports the accuracy. The points were distributed in an 'equalized stratified random' fashion, where half were located in lakes, and half in non-lakes.

Quantitative error assessment for test regions

The error assessment (Supplementary Data Table 4) indicates that for the HMA region, our automated method resulted in 0.05% errors of omission for non-glacial lake area and 11.60% for glacial lakes; and 10.40% errors of commission for non-glacial lakes and 0.05% for glacial lakes. The overall accuracy of the automated method was 94.18%. In other words, the method missed glacial lake pixels about 12% of the time, and identified them mistakenly 0% of the time. We discuss scenarios where the errors may be greater, below.

For the Greenland test region (Supplementary Data Table 5), our automated method resulted in 0.21% errors of omission for non-glacial lake area and 32.32% for glacial lakes; and 24.47% errors of commission for non-glacial lakes and 0.31% for glacial lakes. The overall accuracy of the automated method was 83.73%. In other words, the method missed glacial lake pixels about 32% of the time, and identified them mistakenly 0% of the time. The Greenland test area was chosen as a 'worst case scenario', specifically because the model worked fairly poorly here, with false positives in the ocean (Extended Data Figure 8b). These high errors resulted in more manual editing of Greenland lake outlines.

Sources of error

The most significant sources of error are due to varying water and adjacent terrain properties:

(1) The colour of glacial lakes varies considerably as a function of brash ice or bergy bit content, suspended sediment, and other properties. Brash ice can look like glacier ice, and extremely turbid water can look like wet sediment or wet medial moraine material. Threshold algorithms, which are built to capture the majority of lakes, as described here, sometimes fail to detect some lakes entirely, or more commonly under-size them.

(2) Frozen lake conditions can cause a complete non-detection of the lake, or large underestimation, when using automated methods[69]. This was especially problematic at high latitudes, where the surface of some lakes do not thaw entirely over the summer, or if they do, are ice-free for such a short period that they were not sufficiently imaged by Landsat. This was mostly an issue in the earliest years of our analysis was part of the reason we decided not to include the 1980s data. In later years when warming temperatures meant that lake surfaces were thawed for longer[70], and when satellite imaging was more frequent, these lakes would have been detected and the data complete enough for reliable change assessments.

(3) Shadows from terrain or cloud are another problem due to reduced Digital Numbers, reduced signal-to-noise, and shifted band ratios when the faint illumination is mainly from blue sky. In our case, we used the mean value of each pixel in the stack to reduce shadowing effects.

In favorable cases, where the lake is not frozen, the lake water spectral signature contrasts strongly with non-lake, and there are no cast shadows on the lake, then accuracy can be very high (errors are low), and the chief errors consist of the matters of precision.

Sources of errors unrelated to the optical properties of the lake water and terrain also exist:

(4) Errors due to omissions or inaccuracies in external datasets. The GLIMS/RGIv6.0 glacier database is not perfect and some glaciers are not mapped at all or were much smaller when mapped than in the earlier parts of our Landsat time series; thus, some lakes were missed. Similarly, no DEM is ideal for every situation, and freely available global DEMs are not numerous. The 2000-2010 ASTER GDEM2 (https://asterweb.jpl.nasa.gov/gdem.asp) has gaps, especially at higher latitudes. The 2000 SRTM (https://www2.jpl.nasa.gov/srtm/) terrain model, while more reliable, only extends from 56ºS to 60ºN. Similarly, for lakes near sea level, some DEM pixels were too low, meaning that those pixels in our Landsat mosaic were filtered out since they were 'below' sea level.

Further, since any particular DEM does not necessarily reflect the Earth's surface at the time of Landsat acquisition (especially in glaciated environments), we had to be flexible in our slope threshold since what is covered by lake in the Landsat image may have been glacier ice (and thus steeper) in the DEM. We found that filtering by the median slope across the lake of <10° was a good compromise for glacial lakes.

We combined the ALOS AW3D30 and ViewFinderPanorama DEM (http://viewfinderpanoramas.org/dem3.html) for global coverage, which provided the best compromise for our particular use. However, since we use only a single instance of both the GLIMS database and the DEM, lakes that may exist in regions that are poorly covered will be omitted in *all* time-steps, and thus will not unduly influence the time series. In our publicly available Google Earth Engine scripts, users can select different DEMs.

(5) Human error in digitizing lake outlines also occurs[2], though probably is less than errors associated with digitizing glaciers, especially debris-covered ones.

(6) In some cases, a lake's centroid differs between different time steps, and as a result, the coordinate ID may differ, making tracking individual lakes difficult. For example, if a lake was bisected due to a striping artefact (SLC-off Landsat 7), it would have a centroid closer to the glacier, and possibly a second centroid farther away (in effect producing two lakes). If the more distal lake was then >1 km from the nearest glacier, it would not be counted, reducing the overall area of mapped lakes. We cannot eliminate the Landsat 7 striping issue, but minimize it by combining images from various sensors into the mosaic. Similarly, if a lake expanded substantially between two time steps, the centroid may have migrated sufficiently to have a

different ID. Our centroid coordinate ID is based on the decimal degree latitude and longitude to two decimal places, which was seen as a good compromise, reducing the likelihood of having adjacent lakes with the same ID (which would be more likely if rounded to one decimal place). In our test area in HMA (Extended Data Figure 6), one large lake was mapped accurately in all methods, but its centroid was slightly different between the methods. As a result, there are circles at about 3.9 km^2 on the X and Y axes in Extended Data Figure 9c, representing the mismatch between centroid IDs in the manual vs automatically mapped lakes.

Volume-area scaling

Since glacial lake bathymetry is difficult, expensive, and dangerous to determine, some authors[34] have related lake area to volume using empirical equations. Supraglacial lakes can lengthen either up- or down-glacier, widen to either side, and increase in depth (by melting into the ice). Supraglacial lakes may also shrink by drainage, sediment infill, or basin closure by ice creep. Moraine-dammed lakes on the other hand, are constrained by end and lateral moraines and so grow mainly in length as the ice retreats (or shrink if the glacier advances into the lake), and possibly in depth as the lake either melts deeper into relict ice on the lakebed or as the lake grows upvalley into a basin beneath the retreating glacier; and outlet incision of the moraine dam may lower the lake level, area, and volume. Lakes that have become detached from their glaciers do not tend to grow very much in any direction[56], but rather they may slowly fill with sediment or lower due to outlet incision.

Cook and Quincey[34] found that different lake types (e.g. supraglacial, moraine-dammed, and ice-dammed) are characterized by different area-volume relationships: moraine-dammed lakes are characterized by a linear relationship, for example, while ice-dammed lakes exhibit a more exponential curve. However, they found that a combined global dataset of all glacier lake types produced a strong correlation (R^2 of 0.96), between lake area and volume even when using a single (power) relationship. This high R^2 value is not surprising given that volume in general is a direct function of lake area. Importantly, Cook and Quincey[34] demonstrated that a few large lakes can therefore contain significantly more water than many smaller lakes of the same total area. It is important to note that the largest lake in the Cook and Quincey[34] dataset was <20 km^2 in area and so the applicability of their relation to larger lakes is unknown. Very large lakes fronting piedmont glaciers (e.g. Malaspina Lake/Malaspina Glacier, or Vitus Lake/Bering Glacier) may have very different volume-area scaling than smaller lakes that occupy glacial valleys. These large lakes may occupy accommodation space produced by isostatic depression from these large lobes of ice. But at present, no study has investigated this question.

Here, we evaluated lake volume-area scaling using 73 of the data points (lakes) presented by Cook and Quincey[34] (excluding one outlier, Laguna Safuna Alta, and one duplicated lake, Bashakara), combined with an additional 49 lakes (Supplementary Data Table 6). The lake areas in the Cook and Quincey[34] study are much smaller than the areas for some of our newly mapped lakes, and our additions contain observations of larger lakes.

We then recalculated the volume-area scaling by taking a random 75% sample of the combined Cook and Quincey[34] and our data for model training, retaining the remaining 25% for model testing. We then compared two models. The first was a log-log-linear scaling relationship of the form:

$$ln(V) = \beta_0 + \beta_1 ln(A) + \varepsilon \tag{3}$$

Where V is lake volume (x 10^6 m^3) and A is lake area (m^2). β_0 and β_1 are the slope and intercept of the log-log-linear regression scaling, and ε is the random error component. To use the log-log linear scaling to predict volume the relationship in (3) must be back-transformed:

$$V = e^{\beta_0} A^{\beta_1} e^{\varepsilon} \tag{4}$$

Note that in (4), when the prediction is back-transformed to predict volume, the random error component is multiplicative and non-linear. This possibly introduces bias in prediction, particularly for the larger lakes. To compare prediction error and bias we also estimate the non-linear power scaling directly using non-linear least-squares (nls) function in the R Statistical Program[71]:

$$V = k_1 A^{k_2} + \varepsilon \tag{5}$$

The coefficient k_1 is the corollary to the intercept, where $\log(k_1)$ would be the intercept in log-log space. The coefficient k_2 is the corollary to the slope in eq 3. Estimated coefficients are given in Supplementary Data Table 7.

We then predicted volume for the 25% testing subsample for the combined data for each of these models. To compare the models we calculated the root mean squared squared prediction error (RMSPE) as:

$$RMSPE = \sqrt{\frac{\sum (V_i - \hat{V}_i)^2}{q}}, \tag{6}$$

where V_i is the observed volume and $\hat{V}_i$ is the predicted volume for the i^{th} lake in the testing subsample, and q is the number of lakes in the testing subsample (30). We also compare residual plots for each model.

Overall when used to predict volume for the independent testing subset, the non-linear scaling had much lower RMPSE (0.44 km^3) than the log-log-linear scaling (0.98 km^3). However, we noted in the residual graphs that the nonlinear scaling systematically underpredicted volume of smaller lakes, whereas the log-log-linear model did not exhibit such obvious bias (Extended Data Figure 10). In contrast, the log-log-linear scaling severely and systematically overpredicted volume for the larger lakes. The nonlinear scaling showed no such systematic bias. We therefore applied the log-log-linear scaling to lakes $\leq$0.5 km^2 in area (the point where the bias in the log-log linear model is first apparent) and the nonlinear model to lakes >0.5 km^2 (see Supplementary Data Table 7; Eq. 4 and 5). If we compare the RMSPE for only those lakes ≤0.5 km^2, we see that the RMSPE for those small lakes (17 small lakes in testing set) is 0.0005 km^3 for the non-linear scaling, whereas for the log-log linear scaling the RMSPE for the small lakes in the testing set is reduced to 0.0003 km^3. This demonstrates that the multiplicative error in the log-log-linear scaling prediction does not provide substantial bias in the prediction of small lake volume, but rather is an issue for predicting the volume of larger lakes. Relative to the large lakes this is a small contribution to the overall RMSPE in the test data. However, for our final volume prediction globally this bias would be propagated through summing a multitude of small lakes (84% of the lakes globally across all years). We therefore chose a mixed model to predict global glacial lake volume.

We use a Monte Carlo method to quantify uncertainty in predicted lake volumes and to estimate prediction intervals for volume. For lakes $\leq$0.5 km^2 we estimated point predictions for volume using the back-transformed value from the log-log-linear fit (eqn 4). For each lake we then sampled 10^4 random draws from a bivariate normal distribution. The bivariate mean values were entered as the point coefficient estimates $\{\beta_0, \beta_1\}$ (Supplementary Data Table 7), and we used the estimated coefficient variance/covariance matrix for the bivariate normal variance/covariance matrix. This assumes that the coefficients follow a bivariate normal distribution, and preserves in the random draws any relationship between β_0 and β_1

We repeated the process for lakes >0.5 km^2 using the nonlinear scaling. Because the k_1 and k_2 values in this fit have no correlation and the k_1 value is very close to zero, we fix the k_1 coefficient and sample the k_2 coefficient from a univariate normal distribution with the point estimate and associated standard error. For each lake we retain the middle 95% of MC-predicted volumes, and then sum the total volumes by year, first globally and then individually by region and country. For each year we take the bounds of the MC-generated total volumes as a 95% prediction interval (Extended Data Figure 1). Note that the MC predictions for the non-linear scaling have a slight right-skew, which propagate to a prediction interval that is not centered.

Methods only References

59. McFeeters, S. K. The use of the Normalized Difference Water Index (NDWI) in the delineation of open water features. *International Journal of Remote Sensing* **17**, 1425–1432 (1996).
60. Bhardwaj, A. *et al.* A lake detection algorithm (LDA) using Landsat 8 data: A comparative approach in glacial environment. *International Journal of Applied Earth Observation and Geoinformation* **38**, 150–163 (2015).
61. Nie, Y., Liu, Q. & Liu, S. Glacial lake expansion in the central Himalayas by Landsat images, 1990-2010. *PLoS ONE* **8**, e83973 (2013).
62. Rahaman, K. R., Hassan, Q. K. & Ahmed, M. R. Pan-sharpening of Landsat-8 images and its application in calculating vegetation greenness and canopy water contents. *ISPRS International Journal of Geo-Information* **6**, 168 (2017).
63. Zhu, Z. *et al.* Benefits of the free and open Landsat data policy. *Remote Sensing of Environment* **224**, 382–385 (2019).
64. Cooley, S. W., Smith, L. C., Ryan, J. C., Pitcher, L. H. & Pavelsky, T. M. Arctic-boreal lake dynamics revealed using CubeSat imagery. *Geophysical Research Letters* (In press) doi:10.1029/2018GL081584.

65. Stokes, C. R., Sanderson, J. E., Miles, B. W. J., Jamieson, S. S. R. & Leeson, A. A. Widespread distribution of supraglacial lakes around the margin of the East Antarctic Ice Sheet. *Scientific Reports* **9**, (2019).
66. Lea, J. & Brough, S. Greenland's supraglacial lakes increase by a quarter in the last 20 years. in *EGU General Assembly Conference Abstracts 17968* (2020).
67. Chander, G., Markham, B. L. & Helder, D. L. Summary of current radiometric calibration coefficients for Landsat MSS, TM, ETM+, and EO-1 ALI sensors. *Remote Sensing of Environment* **113**, 893–903 (2009).
68. GLIMS and NSIDC. Global Land Ice Measurements from Space glacier database. (2005) doi:10.7265/N5V98602.
69. Korzeniowska, K. & Korup, O. Object-based detection of lakes prone to seasonal ice cover on the Tibetan Plateau. *Remote Sensing* **9**, 339 (2017).
70. Luoto, T. P., Rantala, M. V., Kivilä, E. H., Nevalainen, L. & Ojala, A. E. K. Biogeochemical cycling and ecological thresholds in a High Arctic lake (Svalbard). *Aquatic Sciences* **81**, 34 (2019).
71. R Core Team. *R: A language and environmental for statistical computing.* (2018).
72. Khadka, N., Zhang, G. & Thakuri, S. Glacial lakes in the Nepal Himalaya: Inventory and decadal dynamics (1977-2017). *Remote Sensing* **10**, (2018).
73. Worni, R., Huggel, C. & Stoffel, M. Glacial lakes in the Indian Himalayas — From an area-wide glacial lake inventory to on-site and modeling based risk assessment of critical glacial lakes. *Science of The Total Environment* **468–469**, S71–S84 (2013).
74. Veettil, B. K. *et al.* Glacier changes and related glacial lake expansion in the Bhutan Himalaya, 1990–2010. *Regional Environmental Change* **16**, 1267–1278 (2016).
75. Tadono, T. *et al.* Development and validation of new glacial lake inventory in the Bhutan Himalayas using ALOS 'DAICHI'. *Global Environmental Research* **16**, 31–40 (2012).

Extended Data Figures

Extended Data Figure 1. Point and interval estimates of total global glacial lake volume. Note that the prediction intervals (vertical error bars) have some overlap, with a consistent positive trend. Vertical lines extend to the lower and upper bounds of the 95% Monte Carlo prediction interval. Horizontal dashed lines indicate the time span of each time step in the series.

Extended Data Figure 2. Example of lake shrinkage with retreat of Barnes Ice Cap, Baffin Island, Canada. Lakes visible in 1990-99 are in yellow (or dashed yellow in panel b), while lakes in 2015-18 are in white. In the 1990-99 mosaic shown in panel a, three large lakes (and one smaller) are visible, which by 2015-18 (mosaic in panel b) have changed markedly. The two larger northern lakes shrunk due to terminus retreat exposing an outlet, while the southern lake grew due to terminus retreat. Note that background images are multiyear mosaics constructed from Landsat imagery from 1990-99 (a) and 2015-18 (b).

Extended Data Figure 3. Total glacial lake volume for all affected countries, for all years of record. Vertical dashed line indicates a total volume of 1 km^3, while dash-dot line indicates a total volume of 10 km^3. Thirty-one countries have contained at least one glacial lake over our study period, but twenty-two country totals contain <1 km^3. Volumetrically, the top five countries (Greenland/Denmark, Canada, Chile, United States, Argentina) contained 84% of the world's glacial lake volume (135.5 km^3), and each country held more than 10 km^3 in 2015-18. With 42.7 km^3 in 2015-18, Greenland/Denmark had more glacial lake storage than any other country, with just over a quarter of the world's 2015-18 total (Fig. 3). Canadian lakes contained slightly less, with 36.9 km^3; Chilean lakes contain 16% of the total (25.3 km^3); while US lakes (mostly in Alaska) contain ~12% (18.8 km^3). Argentina has the fifth highest-ranked glacial lake volume in the world, holding ~8% (11.9 km^3) of the 2015-18 total, though if we include the three largest lakes, Argentina would likely be the top ranked country. Generally, lake volume by country increases with time, although there are exceptions.

Extended Data Figure 4. Flowchart of processing steps for automated delineation of glacial lakes. The NDWI and NDSI thresholds for each RGI region are described in Supplementary Data Table 3. Other thresholds applied in Google Earth Engine included surface temperature (≥-1ºC), slope (<40º), elevation (≥5m asl), for each pixel. Any deviations from these values are reported in Supplementary Data Table 3. In the ArcGIS Pro processing chain, we used the 'Eliminate Polygon Part' donut-filling tool, and thresholds for area (0.05-200 km^2), slope (≤10º), and distance-to-glacier (≤1 km) for each polygon.

Extended Data Figure 5. Pixelwise Landsat mosaic (SWIR1-NIR-R) of the test area in Nepal/Tibet (2016-17). Red dashed box in inset map shows approximate extent of main map, and black dashed box in main map shows extent of panels in Extended Data Figure 6.

Extended Data Figure 6. Results from steps in our processing chain for area outlined with black box in Extended Data Figure 4. Panel (a) shows all "lake" polygons from the threshold NDWI/NDSI image (n = 5648 in full extent of Extended Data Figure 4); (b) shows only those polygons with median slope ≤10° (n = 1930); (c) shows those polygons >0.05 km^2 (n = 144); (d) compares the final lake polygons after being filtered for proximity to a glacier (n = 130) (in green) with manually digitized lake polygons (pink) (n = 140). Note the false positives in the northern part of the image. These were removed manually in the analyses presented in the Results but were included for the error analyses in Supplementary Data Table 4. Well-studied Imja Lake and Lower Barun Lake are labelled for reference. Background image is the RGB mosaic for 2015-2016 produced for the error analysis.

Extended Data Figure 7. Pixelwise Landsat mosaic (SWIR1-NIR-R) of the test area in Greenland (2016-17). Red dashed box in inset map shows approximate extent of main map, and black dashed box in main map shows extent of panels in Extended Data Figure 5. Kangerlussuatsiaq Fjord and Maniitsoq ice cap are labelled for reference.

Extended Data Figure 8. Results from steps in our processing chain for area outlined with black box in Extended Data Figure 7. Panel (a) shows all “lake” polygons from the threshold NDWI/NDSI image (n = 2112 in full extent of Extended Data Figure 7); (b) compares the final lake polygons after being filtered for median slope ≤10°, area >0.05 km^2 and proximity to a glacier (n = 36) with manually digitized lake polygons (pink) (n = 35), and RGI/IMBIE glacier outlines in white. Note the false positives preserved after filtering in Kangerlussuatsiaq Fjord, described in the text. These were removed manually in the analyses presented in the Results but were included for the error analyses in Supplementary Data Table 5. Background image is the RGB mosaic for 2016-2017 produced for the error analysis.

Extended Data Figure 9. Summary of results for the demonstration regions (see Extended Data Figures 4, 6): (a) Histogram of total lake count per area bin from automated optical (blue) and manual (red) methods for the HMA test region; (b) Histogram of total lake count per area bin from automated optical (blue) and manual (red) methods for the Greenland test region; (c) Comparison of lake area (km^2) from automated optical against manual methods for both study areas. Vertical and horizontal error bars in (c) are per Haritashya et al.[2]. Note that the error analysis shown here (and in Supplementary Data Table 4, 5) was performed prior to any manual modifications to the automatically mapped polygons. In other words, the raw but filtered output from the model was used. Data points on the X and Y axes represent lake polygons that either changed sufficiently to have different centroid coordinates, or else were not mapped in either the manual or automated procedures.

Extended Data Figure 10. Training and test observed lake area and volume scaling for (a) lakes ≤0.50 km^2 in area, and (b) lakes >0.50 km^2 in area. Estimated models for eq 1 (log-log) and eq 2 (nls) are overlain on the points. Note that the models were estimated for the training data only. The log-log model better predicts volume of small lakes, but over predicts large lakes. The non-linear scaling model under predicts small lakes, but better predicts volume of large lakes. 95% confidence intervals for the final chosen model for each lake size are shown with dashed lines.

****Reviewers & editors: For Supplementary Data Tables please see submitted .xlsx file** Captions provided here for reference.**

Supplementary Data Table 1. Point estimates and 95% prediction intervals for global glacial lake volume, and for select countries and regions

Supplementary Data Table 2. Comparison of select regional and country-level lake estimates.

Supplementary Data Table 3. Regional parameters used for glacial lake mapping in Google Earth Engine

Supplementary Data Table 4 Confusion matrices for optical mapping of glacial lakes in HMA test region.

Supplementary Data Table 5. Confusion matrices for optical mapping of glacial lakes in Greenland test region.

Supplementary Data Table 6. Compiled dataset of glacial lake areas and volumes.

Supplementary Data Table 7 Coefficient estimates and associated total prediction error in test data for log-log-linear and nonlinear scaling of area to volume. Standard errors for each coefficient are given in parentheses. The covariance between the intercept and slope for the log-log-linear model is -0.00496. RMSPE is the square root of the mean squared prediction error for all lakes in the testing data.

Data Availability

The complete lakes database is available at doi: (Note to reviewers: this will be populated with a DOI on publication).

Code availability

Our Google Earth Engine script is available at(https://code.earthengine.google.com/31a9acd31b65796a47f2823572c3307c) Scripts for Monte Carlo estimation of volume from lake area available at https://github.com/mkenn/GlacialLakeMC.git.

Corresponding author: Correspondence and requests should be sent to DHS.

Acknowledgements

Support for this work was provided by NASA (NNX16AQ62G and 80NSSC19K0653) to JSK, UKH, and DHS, and from NSERC (Discovery Grant 2020-04207 and Discovery Accelerator Supplement 2020-00066) to DHS. Without free access of the Landsat data archive, this and many other scientific efforts would not have been possible. #thanksNASA #thanksUSGS

Author Contributions

DHS, JSK, and UKH designed the study and are co-investigators on the NASA grant that funded the work. DHS and AB designed and wrote the Google Earth Engine model with input from ARB, and performed the subsequent data analysis in ArcGIS Pro. CSW provided expert opinion on glacial lake mapping. DHS and AB performed the error analysis on the lake digitizing, while MK performed the volume-area scaling analysis and error assessment. RB and SH contributed interpretations of the data. KS provided manually digitized lake outlines against which to test the method. DHS wrote the paper, with input and editing from all authors. All authors, especially JSK, contributed substantially to the Discussion.

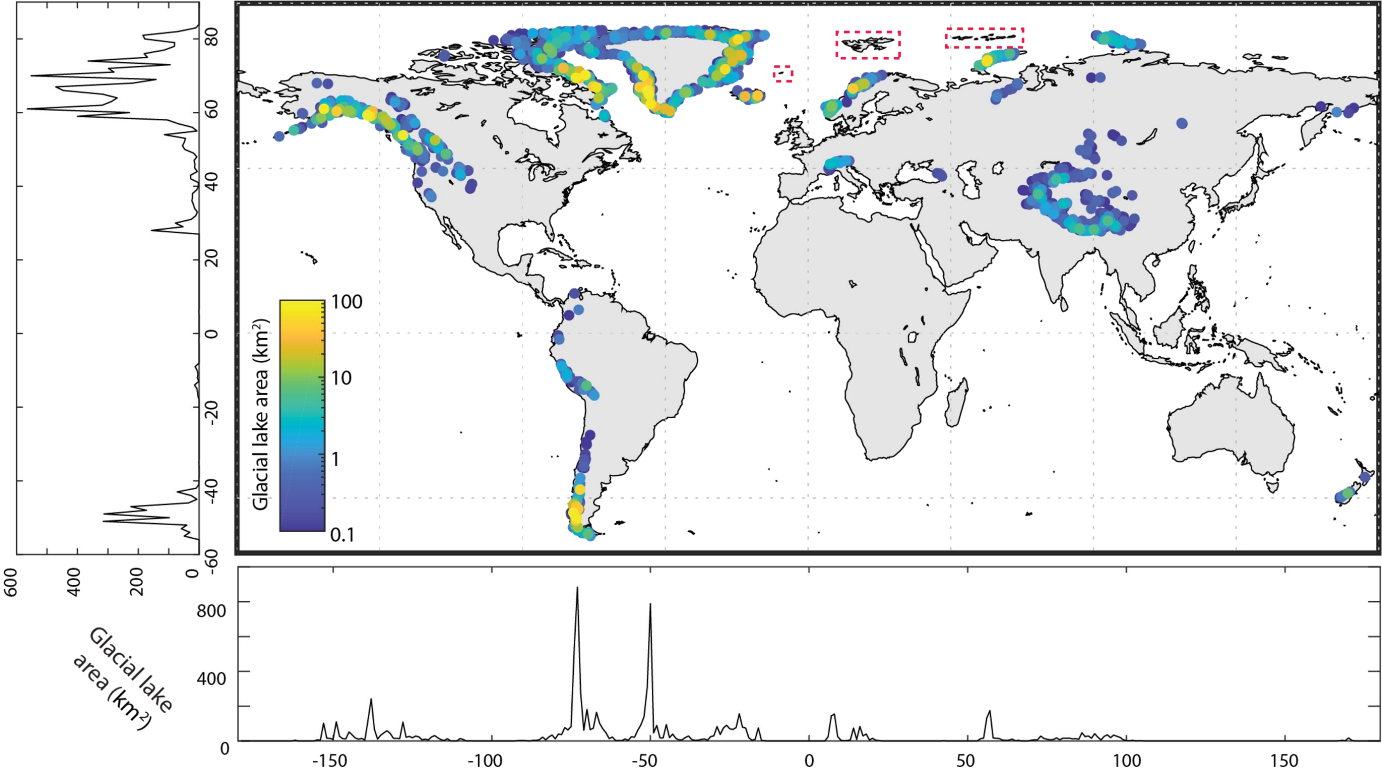

Glacial lake area (km²)
100
10
1
0.1
80
60
40
20
0
-20
-40
-60
600
400
200
0
800
400
0
Glacial lake area (km²)
-150
-100
-50
0
50
100
150

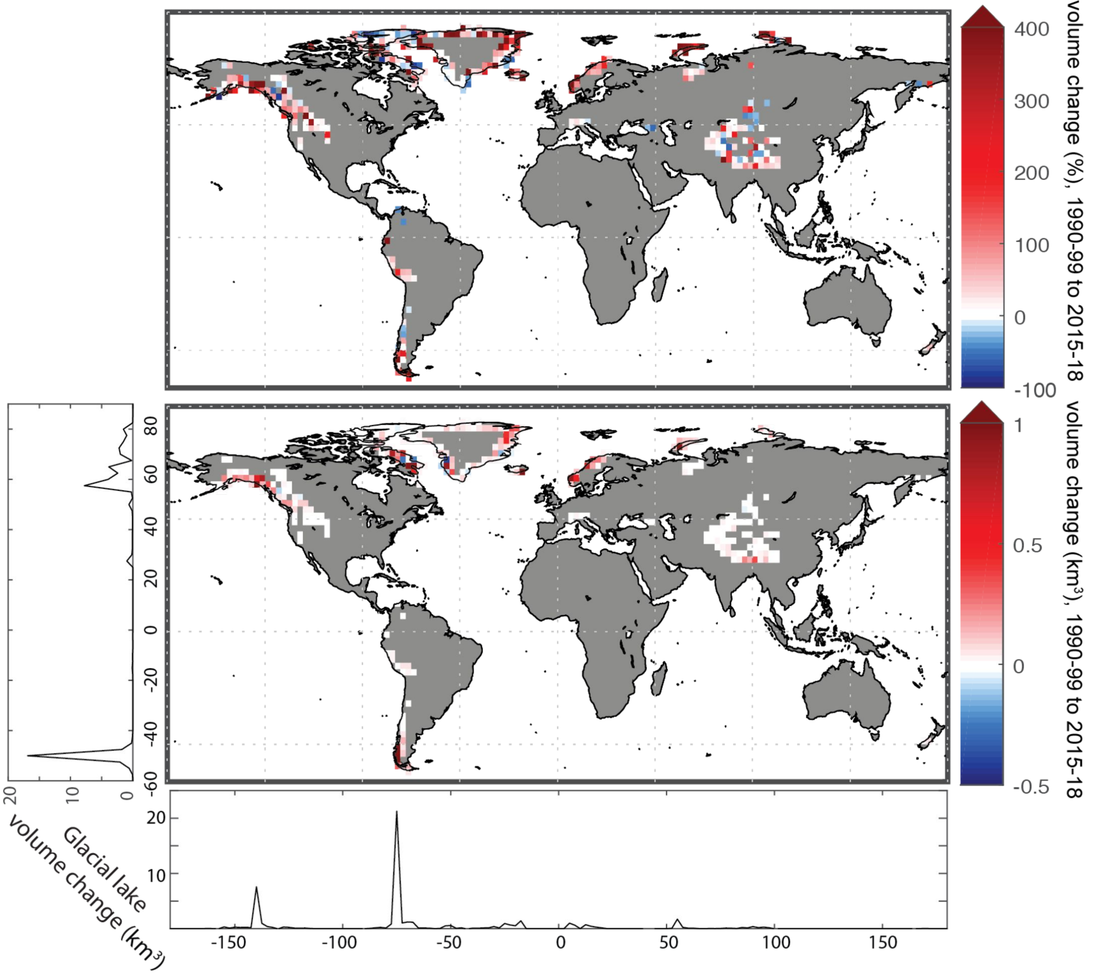

volume change (%), 1990-99 to 2015-18
400
300
200
100
0
-100
volume change (km³), 1990-99 to 2015-18
1
0.5
0
-0.5
80
60
40
20
0
-20
-40
-60
20
10
0
Glacial lake
volume change (km³)
20
10
-150
-100
-50
0
50
100
150

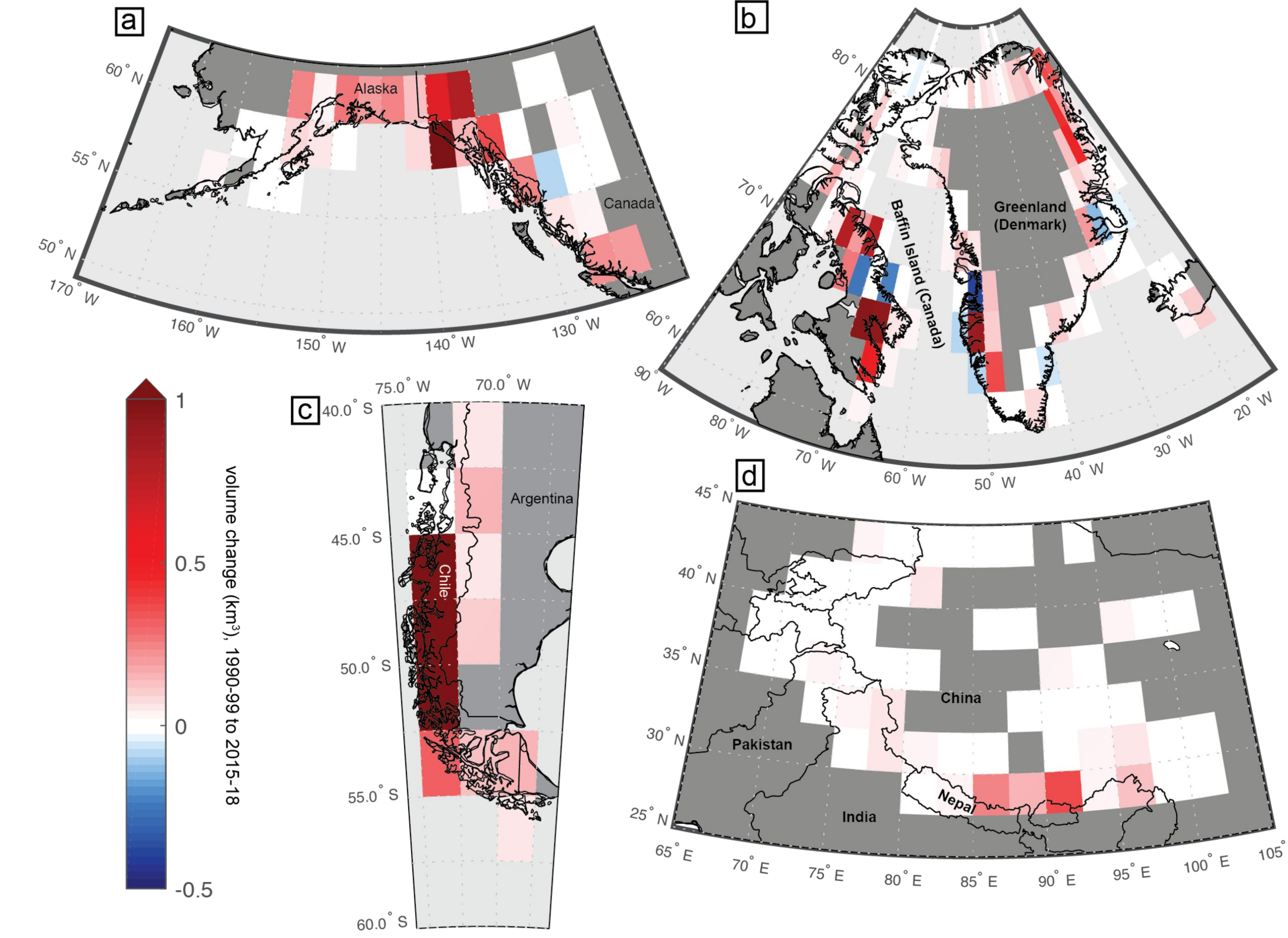
a
b
c
d
Alaska
Canada
60° N
55° N
50° N
170° W
160° W
150° W
140° W
130° W
Baffin Island (Canada)
Greenland (Denmark)
80° N
70° N
60° N
90° W
80° W
70° W
60° W
50° W
40° W
30° W
20° W
Chile
Argentina
75.0° W
70.0° W
40.0° S
45.0° S
50.0° S
55.0° S
60.0° S
China
Pakistan
India
Nepal
45° N
40° N
35° N
30° N
25° N
65° E
70° E
75° E
80° E
85° E
90° E
95° E
100° E
105° E
1
0.5
0
-0.5
volume change (km³), 1990-99 to 2015-18

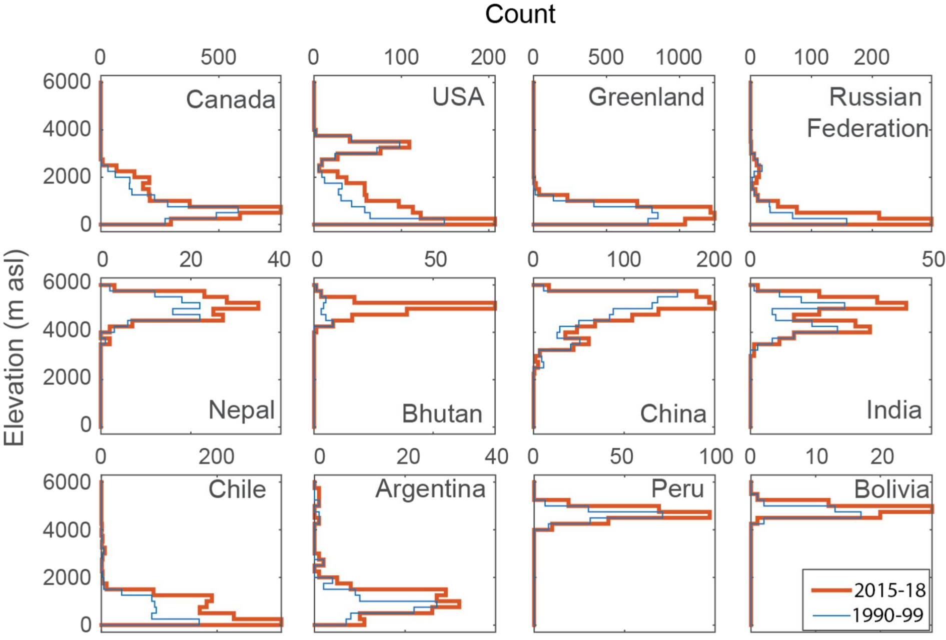

Count
Canada
USA
Greenland
Russian Federation
Nepal
Bhutan
China
India
Chile
Argentina
Peru
Bolivia
Elevation (m asl)
2015-18
1990-99